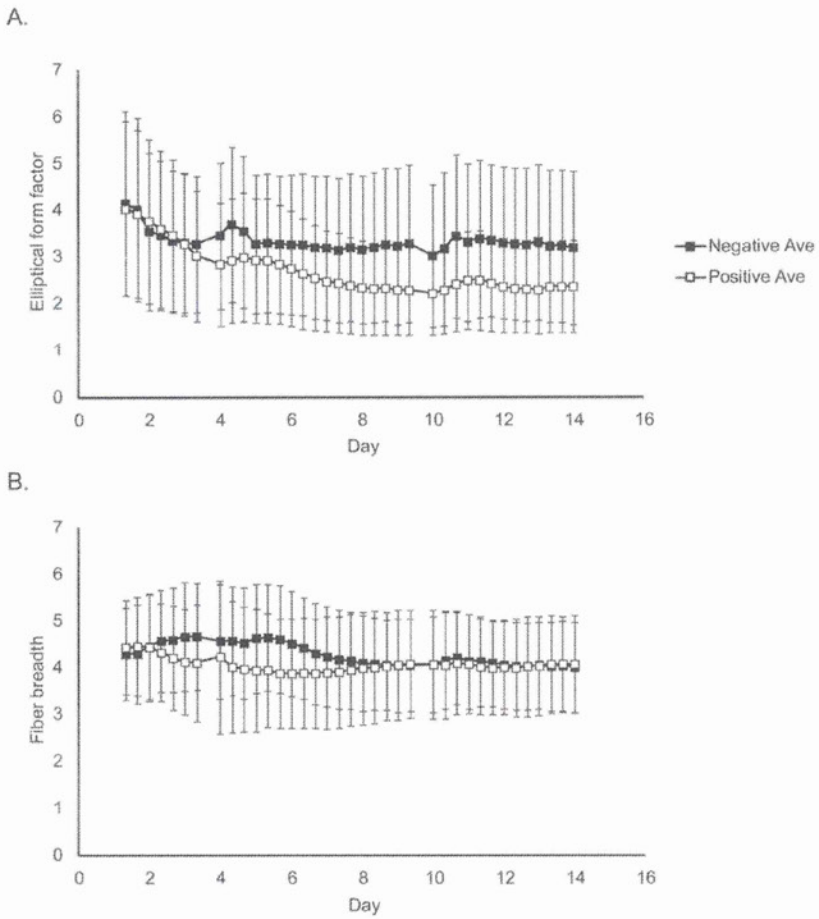

Figure 4. Time series changes of characteristic morphological features. From the 9 morphological features measured, elliptical form factor (A) and fiber breadth (B) of Lot 1 are indicated as representative examples. The symbols indicate the mean value of each morphological feature from all cells in one condition (3 wells ×5 view fields). Roughly, 4,000 to 40,000 cells were measured for the mean. Standard deviations are shown as error bars.
doi:10.1371/journal.pone.0055082.g004

7 day time point, cell morphology in the induction group was observed as flat and spread in multiple two dimensional directions, as compared to the fibroblast-like sharp spindle shape of the control group. By summarizing the quantitative morphological changes in all cells under the same culture conditions through image analysis, an early indication of the cellular phenotype was apparent. For some morphological features, such as Elliptical form factor (the ratio of the object's width to its length) or Fiber breadth (the width of an object modified as a straight fiber), a statistically significant difference ($p<0.01$) between induction and control groups could be identified at a very early culture stage (Fig. 4). Elliptical form factor of Lot 1 was significantly different ($P<0.001$) from day zero at day three of differentiation culture and then throughout the differentiation period. Although these types of morphological differences suggest a relationship to osteogenic induction, they are insufficient to quantitatively predict the final cellular state. To improve predictive power, a machine learning approach was taken to construct a computational model for quantitative prediction and determine the best combination of morphological features to use.

Prediction of osteogenic differentiation potential using multiple and time-course morphological features

Standard practice for bone regeneration therapy is to start by expanding a new patient's cell material to a certain yield, then applies an osteogenic differentiation protocol up until the day of therapy. Variations in the quality of a new patient's starting material can be exacerbated by the stresses of cellular expansion. For these reasons a model for characterizing the regenerative capacity of a patient's cell source, including quality, yield and most importantly osteogenic potential, would add tremendous value to current standard practice.

Two scenarios were designed to simulate anticipated clinical situations available for applying morphology-based prediction models to assess new patient cellular quality. Scenario I: Prediction of new patient BMSC osteogenic potential using a model trained with historical patient data (Fig. 5–A). Scenario II: Prediction of new patient BMSC osteogenic potential using a model trained with historical patient data in addition to data derived from the new patient material (Fig. 5–B). The accuracies of both D14_ALP and D21_Ca models were evaluated in each scenario. Nine morphological features were evaluated from 37 time points over 14 days and complied from 666 image-based input features. The

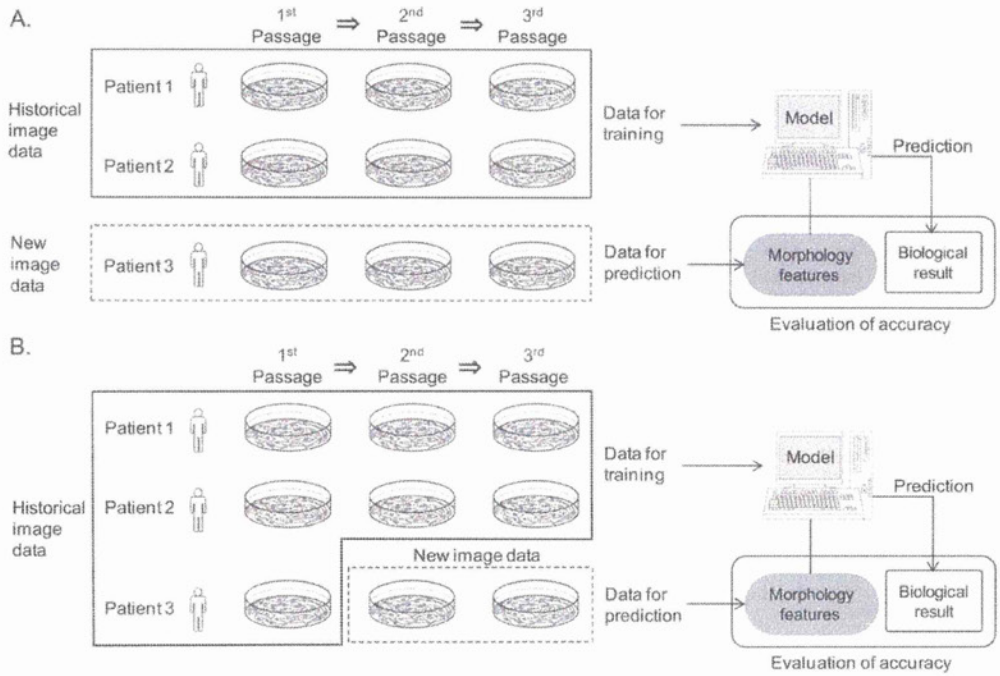

Figure 5. Schematic illustration of two scenarios examined to simulate clinical feasibility. A: (Scenario I) New patient prediction scheme: Trained by historical patient dataset only. Images from all passages of patient 3 were used for prediction. B: (Scenario II) Ongoing patient prediction scheme: Trained by historical patient datasets and a partial dataset from the new patient. For example, for the prediction of cell potential of patient 3, Scheme I uses images of patient 1 and 2 only. Scheme II used images of patient 1 and 2, together with some images from patient 3.
doi:10.1371/journal.pone.0055082.g005

corresponding biochemical differentiation markers from each of the 54 samples were also evaluated. We selected Ridge regression as the machine learning modeling method for linking morphological features to the biomarker measurement results [17]. This method was chosen since Ridge regression is a type of standard regression model that eliminates the multicolinearity problem in multivariate models [18].

Scenario I: New patient prediction scheme. The new patient prediction scheme is designed to simulate the clinical situation where evaluating a new patient's cell quality can be accomplished quickly and reliably (Fig. 5–A). With this scheme, the prediction model can be prepared previously by historical image data from other patients. This model aspires to require no previous data from the new patient.

The prediction accuracies of the D14_ALP and the D21_Ca models are shown in Table 1 and, Fig. 6 (see also Fig. 7 and Table S1 for detailed data). From both prediction results, the correlation coefficients indicated that time-course morphological features of BMSCs during differentiation correlate with the experimentally obtained osteogenic marker values. The average

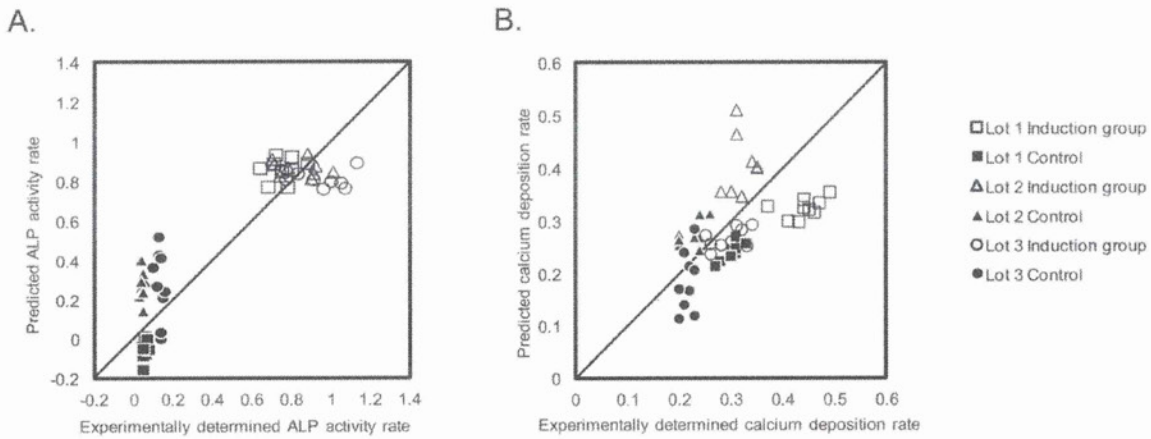

Figure 6. Prediction accuracies in the new patient scheme. A: Scatter plot of experimentally determined values versus predicted values in D14_ALP model, B: Scatter plot of experimentally determined values versus predicted values in D21_Ca model.
doi:10.1371/journal.pone.0055082.g006

Table 1. Prediction accuracy of Ridge regression models for osteogenic differentiation status of hBMSCs.

	New patient prediction scheme		Ongoing patient prediction scheme	
	Ave. absolute prediction error* [−]	R** [−]	Ave. absolute prediction error* [−]	R** [−]
ALP activity rate prediction	0.151	0.903	**0.111**	**0.950**
Calcium deposition rate prediction	0.065	0.526	**0.037**	**0.821**

*Ave. absolute prediction error is the average of the differential between experimentally determined rate and predicted rate.
**Correlation coeffecient between experimentaly determined and predicted rate.
doi:10.1371/journal.pone.0055082.t001

of absolute prediction errors indicates that each prediction model provides predictions within the error rage of ±0.151 with the D14_ALP model and ±0.065 with the D21_Ca model, respectively (Fig. 7). When the variance of all assay data, the result of manual experimental variance, is normalized as 1.0, the prediction errors between different assay measurements can be standardized as 0.194 (D14_ALP) and 0.963 (D21_Ca). This standardized error provides the interpretation that the prediction values are 5-fold stable (D14_ALP) or nearly equal (D21_Ca) compared to the human assay variances.

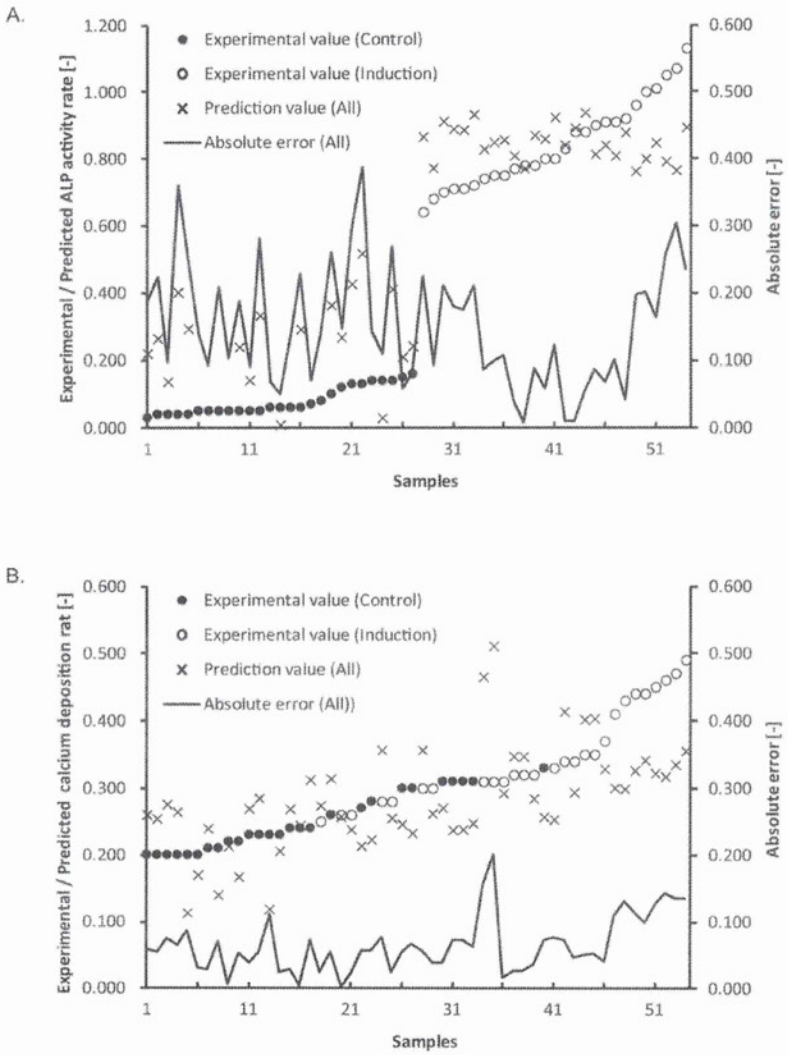

Figure 7. Detailed prediction results in new patient scheme. A: Prediction results and error range in the D14_ALP model. B: Prediction results and error range in the D21_Ca model. All the plotted data were rearranged in the order of experimental values.
doi:10.1371/journal.pone.0055082.g007

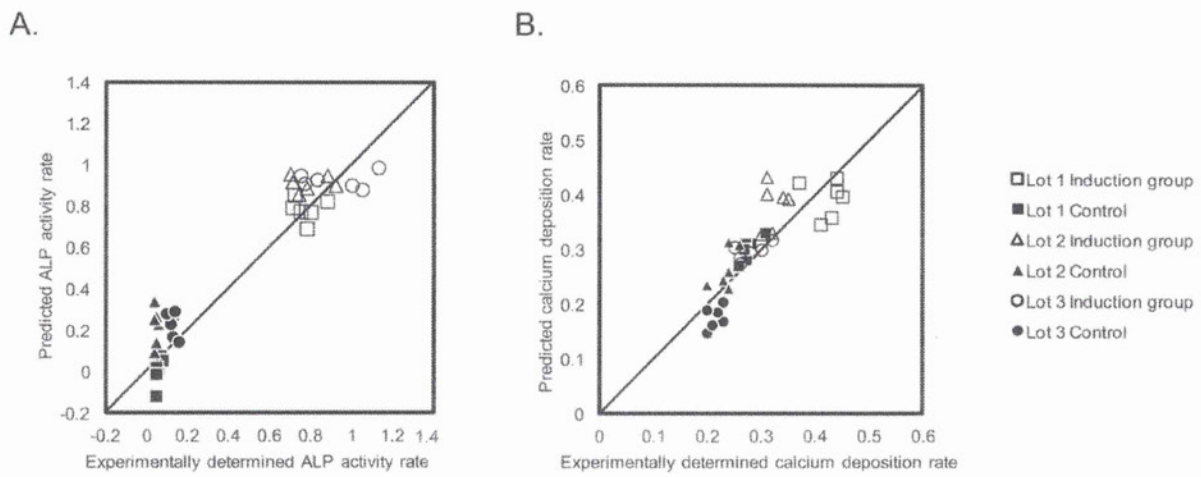

Figure 8. Prediction accuracies in the ongoing patient scheme. A: Scatter plot of experimentally determined values versus predicted values in D14_ALP model, B: Scatter plot of experimentally determined values versus predicted values in D21_Ca model.
doi:10.1371/journal.pone.0055082.g008

Scenario II: Ongoing patient scheme. The ongoing patient prediction scheme is designed to simulate the clinical situation of evaluating a new patient's cell quality with higher accuracy in return for additional data acquisition process (Fig. 5–B). With this scheme, a small sample of the new patient's cells should be differentiated for 14 days as a pilot culture in parallel to the expansion culture. During this pilot culture, cell images are taken to represent the new patient's cellular characteristics. The new patient's data and previous patients' historical data are combined for training the prediction model. Using image data from the next passage and from the 14 day differentiation culture, a prediction can be made prior to the cell harvest (Fig. 5–B). The advantage of this scheme is inclusion of new patient data at the cost of acquiring and inputting new patient images. Characteristics, which may be unique to the new patient, can then be incorporated into training the model with the expectation of a greater predictive value.

The prediction results of the D14_ALP and D21_Ca models are shown in Table 1 and Fig. 8 (see also Fig. 9 and Table S2 for detailed data). These results confirm that the morphological features of hBMSCs observed during differentiation culture highly correlates with the future osteogenic potential. The error ranges were tightened to ± 0.111 with D14_ALP model, and ± 0.037 with D21_Ca model (Fig. 9) as compared to using only historical data to train the model. The standardization of all assay variances to 1.0 results in prediction errors of 0.110 (D14_ALP) and 0.333 (D21_Ca) respectively. Overall, these results suggest that prediction values from Scenario II morphology-based models are nearly 9-fold stable (D14_ALP) or 3-fold stable (D21_Ca) compared to the human assay variances.

When comparing the two scenarios, the prediction accuracies in both prediction models (D14_ALP and D21_Ca) greatly improved in Scenario II, the ongoing patient prediction scheme. These results indicate that incorporation of morphological characteristics from the patient's own cells is extremely important and informative for predicting an individual's BMSC osteogenic potential.

Discussion

Although qualitative cellular morphology is used as a guide for estimating osteogenic differentiation, a quantitative relationship between cellular morphology and biochemical osteogenic markers is not well established. In the present study, we investigated the possibility of predicting osteogenic differentiation of hBMSCs from phase contrast images alone. Specifically, a machine learning algorithm was used to train 14 day cell morphology information and terminal osteogenic biochemical marker values into a model used to predict the terminal marker values from a test set of morphologic data. Our results provide evidence that using this approach can potentially automate and improve decisions, which are currently based on conventional destructive assays and qualitative microscopic assessments.

Using both ALP activity and calcium deposition rates in assessing cellular quality is important to current standard practices. Our proposed modeling schemes allow for accurate prediction of both endpoints. Of particular importance is the accurate prediction of calcium deposition, which is more closely associated with *in vivo* bone formation. For these reasons, constructing different types of prediction models to allow real-time evaluation of the same target cells with multiple aspects and add information for more careful decision making in the culture process. These attributes of an automated computational approach for assessing cellular quality support improvement of safety, efficacy and more rapid and economical scheduling decisions by physicians.

New technology allowing automated image acquisition, which can currently provide more images with greater quality and fewer biases, improves our ability to generate more predictive models based on cellular morphology. In our work, state-of-the art imaging platform (in this study BioStation CT), is the first enhancement technology which lead us to provide uniform and objective data without need for manual optimization of lighting, focusing, or other systematic errors common to manual image acquisition. Operator bias for field selection is also greatly reduced by optimization of the seeding protocol to improve cell distribution together and optimization of the number of fields to view jointly. Image processing biases, the thresholding bias to extract cells from non-cell objects recognized in the images, are also improved by a new automated threshold determination algorithm (data not shown). By preparing three different cell lots and three different passages for cell samples, we aimed to reduce biases of specific patient.

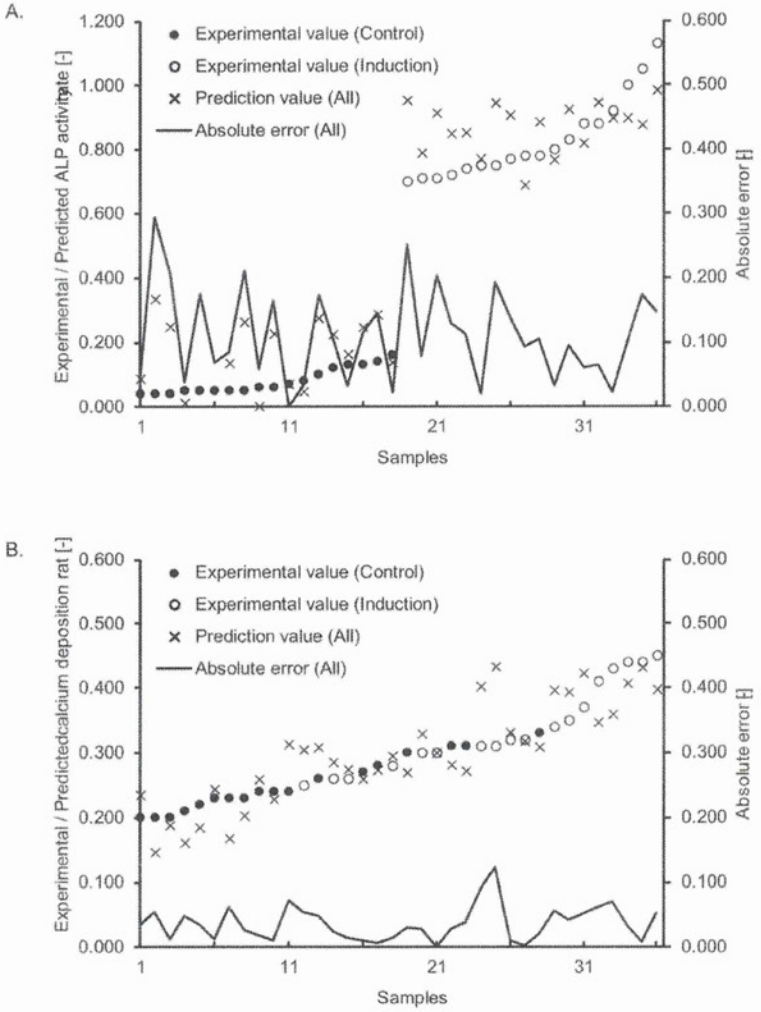

Figure 9. Detailed prediction results in ongoing patient scheme. A: prediction results and error range in the D14_ALP model. B: Prediction results and error range in the D21_Ca model. All the plotted data were rearranged in the order of experimental values.
doi:10.1371/journal.pone.0055082.g009

Table 2. Prediction accuracy of Redge regression models with elimination of each individual features for ALP activity rate.

	New patient prediction scheme		Ongoing patient prediction scheme	
Excluded parameter	**Ave. prediction error* [−]**	**Standardized error** [−]**	**Ave. prediction error* [−]**	**Standardized error** [−]**
Breadth	0.131	0.142	0.078	0.057
Elliptical form factor	0.121	0.124	0.074	0.052
Fiber breadth	0.156	0.197	0.091	0.074
Fiber length	0.136	0.147	0.074	0.051
Hole area	0.141	0.152	0.085	0.060
Inner radius	0.138	0.146	0.088	0.065
Relative hole area	0.134	0.148	0.090	0.065
Shape factor	0.148	0.180	0.108	0.104
Total area	0.136	0.153	0.087	0.064

*Ave. prediction error is the average of the differential between experimentally determined rate and predicted rate.
**Standardized error is calculated by dividing the average of squared errors by variance of all the experimentally evaluated values.
doi:10.1371/journal.pone.0055082.t002

Table 3. Prediction accuracy of Redge regression models with elimination of each individual features for calcium deposition rate.

	New patient prediction scheme		Ongoing patient prediction scheme	
Excluded parameter	**Ave. prediction error* [−]**	**Standardized error** [−]**	**Ave. prediction error* [−]**	**Standardized error** [−]**
Breadth	0.065	0.924	0.028	0.187
Elliptical form factor	0.066	0.972	0.026	0.166
Fiber breadth	0.062	0.870	0.026	0.158
Fiber length	0.065	0.921	0.027	0.164
Hole area	0.065	0.937	0.026	0.138
Inner radius	0.063	0.892	0.028	0.180
Relative hole area	0.060	0.769	0.025	0.146
Shape factor	0.067	0.939	0.029	0.201
Total area	0.067	0.968	0.027	0.160

*Ave. prediction error is the average of the differential between experimentally determined rate and predicted rate.
**Standardized error is calculated by dividing the average of squared errors by variance of all the experimentally evaluated values.
doi:10.1371/journal.pone.0055082.t003

The second enhancement incorporated into this study is the incorporation of robust and continuous morphological features. In this study, it is a key that the morphological features actually used in our modeling are statistical composites (average and standard deviation) of features obtained from all cells from a given condition, which is typically comprised of approximately 4,000–40,000 cells from 15 images for each condition. Such large number of technical replicates offers robustness in each parameter, and effectively enhanced the performance of our prediction model. The continuous image acquisition with precise timing by BioStation CT allowed us to obtain both static morphological features and their dynamic changes throughout the differentiation process. Since morphological changes during osteogenic induction are time-dependent events, it is important to analyze morphological changes with precise timing.

The third enhancement provided by our work stems from the examination of two clinically plausible scenarios. Through these experiments, we found that prediction accuracies of both osteogenic potential measurements greatly increase when the model incorporates training information from early images from the same patient, which reflects individual characteristics in cell morphology. Carefully considering patient-to-patient morphology variation exposes limitations in the current practice of experience-based assessment by culture experts. As indicated in our results, use of new high-content information databases from images, where large amounts of data can be computationally organized and retrieved, is one possible approach for incorporating many aspects related to patient-to-patient variability. Constructing predictive models using historical databases and individualizing new patient predictions by incorporating each new patient's data would be a practical approach to mitigating patient variability while improving the precision of quality assessments.

Comparing the prediction errors of D14_ALP and D21_Ca models in Table 1, the D14_ALP prediction accuracy was higher. One possible explanation for the discrepancy between D14_ALP and D21_Ca predictions is the lack of morphological data during the calcium deposition period, which requires an additional week of culture following two weeks of induction culture. We plan to further investigate ways to enhance predicting this late maturation marker by accumulating more culture images to accrue a larger historical data set. However, we were surprised to discover that without the last seven days of morphology data the D21_Ca model could still predict the final calcium deposition result with reasonable accuracy. To our knowledge, no other reports have been able to accurately estimate the final calcium deposition from early images.

Previous reports have indicated that morphological parameters, similar to the ones used in this study such as flatness or polygonal rate, highly correlate with the osteogenic differentiation potential. Consistent with these reports, we looked at the contribution of each parameter to the prediction performance. In regression analysis, one can examine the effect of each parameter by examining the regression coefficients. Interestingly, among the nine parameters introduced into the regression analysis, there were few sizeable positive or negative coefficients (data not shown). This suggests that there are few dominant morphological parameters that simply correlate to the differentiation potential. Furthermore, when individual features were intentionally eliminated from the model, no significant deterioration was observed in the prediction accuracy (Table 2 and 3). These results suggest that correlation of morphological features and the osteogenic differentiation potential is so complex that there are various compensatory features. Therefore, we conclude that to gain the most robust prediction model for hBMSC osteogenic differentiation potential, all available morphological features throughout the differentiation culture should be incorporated, and biased or feeling-based morphological feature selection should be avoided.

In this work, longitudinal morphological measurements were used as individual, unconnected features, like snapshots. However, to improve the accuracy of the D21_Ca model, we examined ways to incorporate time dependent changes of individual features. With this idea, the same morphological features were converted to change rates between sampling times, analogous to measuring the differences through snapshots. As a result, this morphological feature transformation reduced the D21_Ca model standardized error rate from 0.333 to 0.192 (data not shown). We plan to further investigate the transformation or repeated measurements into time-based trends and patterns in morphological data to improve predictive performance. Our next investigation is designed to further demonstrate applicability and robustness of our proposed method by evaluating the model's ability to characterize "cellular variances", derived from patient diversity, culture protocol effects, and accumulating stresses throughout culture. We also plan to further expand the scope of this work to translate progress made using *in vitro* models and endpoints for morphological prediction of osteogenic potential *in vivo*.

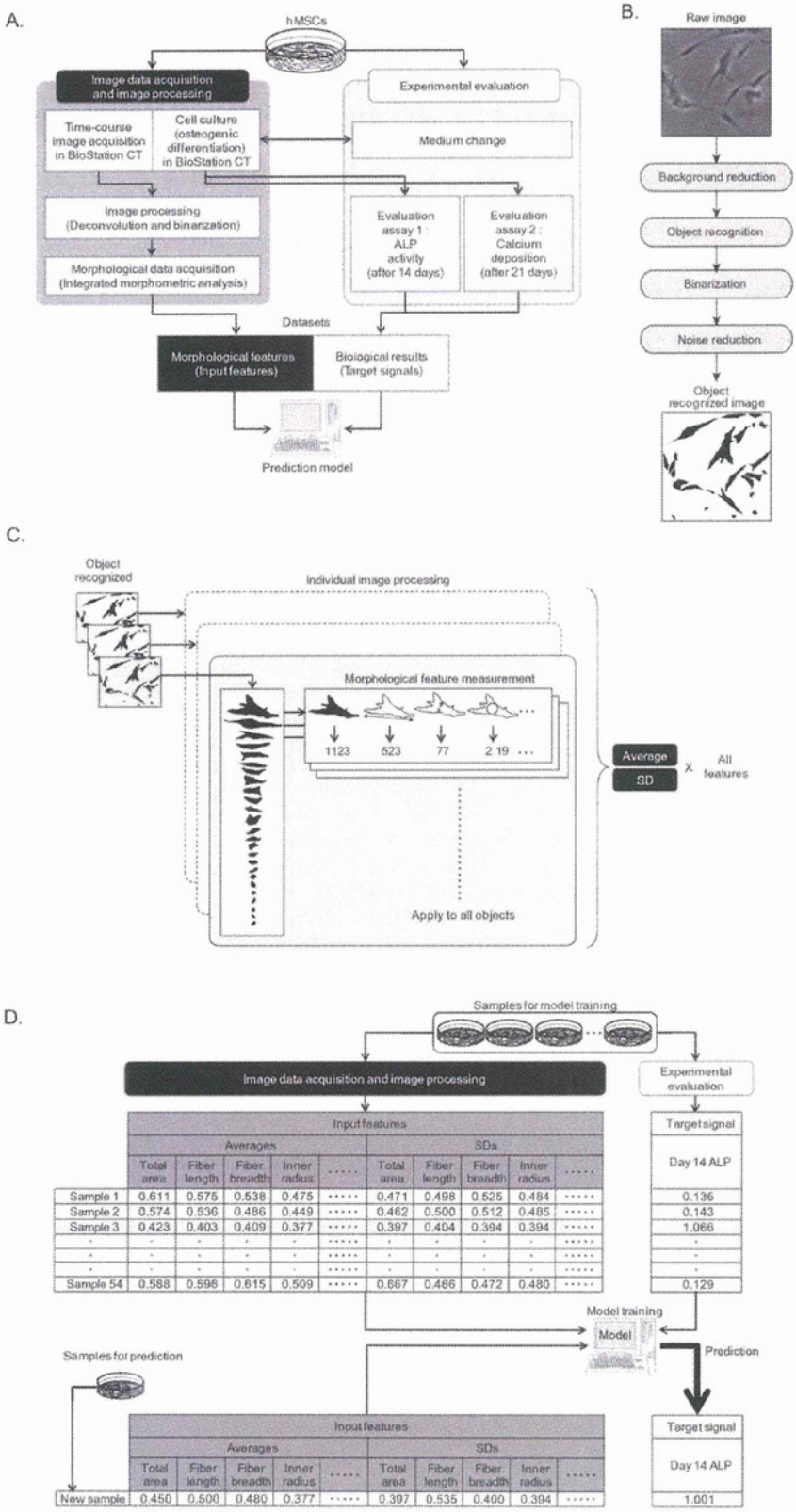

Figure 10. A: Schematic illustration of cell image processing. The raw images were first pre-processed by background reduction processing

by deconvolution and open-close filters. Then, images were binarized by the optimized threshold. The noisy objects were eliminated by particle deletion filter. B: Schematic illustration of cell morphology measurements and data processing. In all object recognized images, all existing objects were measured for the 9 morphological features. Since 1 condition was designed to consist of 3 wells ×5 view fields, all the corresponding object measurement results were processed as a same sample. The average and standard deviation within one sample of all morphological features at each time point were used as the input features for modeling. C: Schematic illustration of prediction model construction. Prediction of differentiation potential consisted of two steps. First, two types of prediction models (D14_ALP model or D21_Ca model) were constructed with the set of image data and experimental evaluation. Second, the values of D14_ALP or the D21_Ca were predicted from the input features of the sample targeted for prediction. The predicted biological rates are compared to the experimentally-determined results to evaluate the accuracy of prediction model.
doi:10.1371/journal.pone.0055082.g010

Materials and Methods

Cells and cell culture

Human bone-marrow derived mesenchymal stem cells (hBMSCs) (Lonza Walkersville, Inc., Maryland, U.S.A.) were subcultured (passaged) in Dulbecco's modified Eagles' medium (DMEM) containing 10% fetal bovine serum (FBS) (Life Technologies Japan Ltd., Tokyo, Japan). Three lots of hBMSCs were designated as Lot 1 (strain number 15000-1, unknown race, Male, 19-year-old), Lot 2 (strain number 17174, Oriental, Male, 20-year-old), and Lot 3 (strain number 11533, Black, Male, 22-year-old), respectively. Lot 1 and 2 were cultured to passages 3, 4, and 5, and Lot 3 was cultured to passages 6, 7, and 8, and cryopreserved for the start of the image acquisition experiment. Cryopreserved cells were seeded at a density of 1.0×10^4 cells/well in 12-well plate (Greiner Bio-One., Frickenhausen, Germany), and the cell-seeding day was designated as day 0 in the image acquisition experiment.

Fig. 1 illustrates the experimental scheme for hBMSC osteogenic differentiation culture. From day 0 to 3, cells were cultured in 10% FBS-containing α-modified Eagle's medium (αMEM) (Sigma-Aldrich Co., St. Louis, MO, U.S.A.). From day 4 to 18, cells were divided into two groups: (1) Osteogenic induction group (Induction, N = 6) and (2) Non-induction group (Control, N = 6). For the induction group, the medium was switched to induction medium consisting of 10% FBS-containing αMEM medium supplemented with 10 nM dexamethasone (Sigma-Aldrich Co.), 100 mM ascorbic acid (Wako Pure Chemical Industries, Ltd., Osaka, Japan), and 10 mM glycerol 2-phosphate sodium salt hydrate (Sigma-Aldrich Co.). For the non-induction group, supplements were not added to the 10% FBS-containing αMEM medium. The appropriate medium was changed at day 7 and day 13. For half of the samples in each experimental group (n = 3), alkaline phosphatase (ALP) activity were quantified on day 18. The remaining samples continued culture until day 25, and calcium deposition was quantified on day 25.

Image acquisition

Figs. 1 and 10-A illustrates the image acquisition scheme during hBMSC osteogenic differentiation culture. From day 0 to day 13 (14 days), phase contrast microscopic images of hBMSCs were obtained using the BioStation CT (Nikon Corporation, Tokyo, Japan). BioStation CT is an automatic cell maintenance system, which maintains a stable incubation environment (37°C, 5% CO_2, 100% humidity) with scheduled automatic image acquisition. The number of view fields was optimized to five, which provides the least error for estimating the correct cell seeding for each well. Five view fields (center position and four positions 2.2 mm from the center) of phase contrast images were acquired from each well with fully automatic focusing. The phase contrast images had the least noise and background when using the halo-reduction lens. Image acquisition timing was set to every 8 hours from day 4 to 18 (magnification = 10x). Time points are designated as time 0 to 38, indicating each of the 8 hour imaging intervals. Data at time 0 was omitted, since the cells were not fully settled. Data at time 7 and time 26 were also omitted, since it was concurrent with medium changes for each well plate, resulting in 36 time-points as a total.

Quantification of ALP activity

Quantitative ALP activity assays were performed as previously described [9]. After 18 days of culture, cell number was measured using a cell counting kit-8 (WST-8®; Dojindo Laboratories, Kumamoto, Japan), and ALP activities were measured with a p-nitrophenyl phosphate solution (Lab Assay ALP®; Wako Pure Chemical Industries, Ltd.). Briefly, for cell count, 100 µl of WST-8 was added to each well containing 1 mL of fresh medium, incubated for 1 hour, and absorbance was read at 450 nm. After WST-8 analysis, each well was washed twice with phosphate buffered saline (PBS) and 800 µL of p-nitrophenyl phosphate solution was added to each well. After 10 min of incubation at 37°C, the conversion to p-nitrophenol was stopped with 800 µl of 3N NaOH and the absorbance of p-nitrophenol was measured at 405 nm. Alkaline phosphatase-specific activity is expressed as p-nitrophenol absorbance (OD; 405 nm)/WST-8 absorbance (OD; 450 nm).

Calcium deposition quantification

After 25 days of culture, cells were fixed with 70% ethanol for 1 hour, washed, and stained for 10 min with 40 mM alizarin red S solution (pH: 4.2). After washing with PBS, plates were incubated with 10% cethylphridinium chloride for 15 min. Thereafter, supernatants were collected from each well and the absorption of each supernatant was measured at 405 nm to determine the amount of calcium deposition.

Cell image processing

All images (.bmp files) were processed by MetaMorph (Molecular device, CA, U.S.A) with the original combination of image-processing filter sets (Fig. 10–A). Briefly, the raw images were pre-processed by open-close filters and binarized by the optimized threshold. All image data was pre-processed using the same brightness threshold, which was optimized by 20 randomly picked image samples. This pre-processing step minimized error between the manually determined image cell number and the number of objects determined after pre-processing. After binarization, all individual objects in each image, consisting of cells and noise (non-cell objects), were measured by the integrated morphometric analysis function to measure morphological features (9 morphological features are: Breadth, Elliptical form factor, Fiber breadth, Fiber length, Hole area, Inner radius, Relative hole area, Shape factor, Total) (Fig. 10–B). The morphological features were carefully selected with the MetaMorph measurement function by logical selection. Features related to color and brightness were excluded first. Second, independent features were selected by hierarchical clustering and highly correlated features ($R>0.85$) were excluded. From the data consisting of object ID and its standardized 9 morphological features (average = 0, standard deviation = 1), the noise data (non-cell objects) was automatically cleansed by the original noise-reduction algorithm

prior to the analysis (patent pending). From the pre-processed data, average (AVE) and standard deviation (SD) from each of the 9 morphological features was calculated from each of the cell objects covering five view fields from the same well, and used as the 18 inputs (9 features with AVE and SD) for each sample to be used in further analysis (Fig. 10–C). The morphological features and cell number (AVE and SD for 19th and 20th feature) from each well were then tagged with the target signals, which are experimentally determined values, resulting in 54 samples (= 3 lots ×2 induction conditions ×3 passages ×3 wells) tagged with ALP values, and 54 samples tagged with calcium deposition values. This process links the "result" (biological measurement) with the "indication" (image-derived morphological feature), to derive a dataset for further modeling (Fig. 10–D).

Construction and evaluation of prediction model

Prediction of differentiation potential consists of two steps (Fig. 10–D): one is the construction of a prediction model, and the other is the evaluation of the constructed model. Using Ridge regression, two types of prediction models were constructed: (1) D14_ALP model, and (2) D21_Ca model. For the new patient scheme, prediction models were trained with 36 samples from 2 lots, and 18 samples from the remaining single lot were predicted. For the ongoing patient scheme, prediction models were trained with 42 samples from 2 lots of 3 passages plus the samples from new lot of 1 or 2 passages were used for training, and 12 samples from the remaining 1 lot were predicted (Fig. 5). The detailed modeling process is described in a previous report (See Section 3 in [18] for details of the Ridge regression method). The performance of each of the models and datasets were evaluated by the average accuracy resulting from leave-one-out cross validation.

For the evaluation of our proposed scheme, two evaluation indices are introduced in our work. One index is the correlation coefficient (R) of actual assay values and prediction values, which evaluates the prediction accuracy and its data coverage. The higher R increases, the more the model is capable of predicting "differentiation marker values" with small error rate. The other index of evaluation that we introduced is the average of absolute error. This value is calculated by obtaining absolute values of (experimentally determined value minus the predicted value). To compare these errors, we standardized these errors by dividing the variance of total experimentally determined values in one assay.

Supporting Information

Table S1 * Exp. determined rate is the abbreviation of the experimentally determined rate.
(XLS)

Table S2 * Exp. determined rate is the abbreviation of the experimentally determined rate.
(XLSX)

Acknowledgments

We are grateful to Mai Okada and Yurika Nonogaki for supporting the experiments and data storage. We also thank Wakana Yamamoto, Yoshihide Nagura, Kazuhiro Mukaiyama, Kenji Kojima, Hiroto Sasaki, and Asuka Miwa for establishing basal analysis protocol and algorithms for image analysis procedure.

Author Contributions

Conceived and designed the experiments: FM HK HA RK. Performed the experiments: FM. Analyzed the data: IT FM RK. Contributed reagents/materials/analysis tools: HS YK HH RK. Wrote the paper: FM IT HK HA RK.

References

1. Wu Y, Chen L, Scott PG, Tredget EE (2007) Mesenchymal stem cells enhance wound healing through differentiation and angiogenesis. Stem Cells 25: 2648–2659.
2. Chen L, Tredget EE, Wu PY, Wu Y (2008) Paracrine factors of mesenchymal stem cells recruit macrophages and endothelial lineage cells and enhance wound healing. PLoS ONE 3: e1886.
3. Barry FP, Murphy JM (2004) Mesenchymal stem cells: clinical applications and biological characterization. Int J Biochem Cell Biol 36: 568–584.
4. Hayashi O, Katsube Y, Hirose M, Ohgushi H, Ito H (2008) Comparison of osteogenic ability of rat mesenchymal stem cells from bone marrow, periosteum, and adipose tissue. Calcif Tissue Int 82: 238–247.
5. Mizuno D, Kagami H, Mizuno H, Mase J, Usami K, et al. (2008) Bone regeneration of dental implant dehiscence defects using a cultured periosteum membrane. Clin Oral Implants Res 19: 289–294.
6. Olivo C, Alblas J, Verweij V, van Zonneveld AJ, Dhert WJ, et al. (2008) In vivo bioluminescence imaging study to monitor ectopic bone formation by luciferase gene marked mesenchymal stem cells. J Orthop Res 26: 901–909.
7. Kagami H, Agata H, Tojo A (2011) Bone marrow stromal cells (bone marrow-derived multipotent mesenchymal stromal cells) for bone tissue engineering: Basic science to clinical translation. Int J Biochem Cell Biol. 43: 286–289.
8. Dennis JE, Esterly K, Awadallah A, Parrish CR, Poynter GM, et al. (2007) Clinical-scale expansion of a mixed population of bone-marrow-derived stem and progenitor cells for potential use in bone-tissue regeneration. Stem Cells 25: 2575–2582.
9. Agata H, Asahina I, Yamazaki Y, Uchida M, Shinohara Y, et al. (2007) Effective bone engineering with periosteum-derived cells. J Dent Res 86: 79–83.
10. Platt MO, Wilder CL, Wells A, Griffith LG, Lauffenburger DA. (2009) Multipathway kinase signatures of multipotent stromal cells are predictive for osteogenic differentiation: tissue-specific stem cells. Stem Cells. 27:2804–2814.
11. Kelly DJ, Jacobs CR (2010) The role of mechanical signals in regulating chondrogenesis and osteogenesis of mesenchymal stem cells. Birth Defects Res C Embryo Today. 90:75–85.
12. Kino-Oka M, Maeda Y, Sato Y, Maruyama N, Takezawa Y, et al. (2009) Morphological evaluation of chondrogenic potency in passaged cell populations. J Biosci Bioeng.107:544–551.
13. Carpenter AE, Jones TR, Lamprecht MR, Clarke C, Kang IH, et al. (2006) CellProfiler: image analysis software for identifying and quantifying cell phenotypes. Genome Biol. 7: R100.
14. Misselwitz B, Strittmatter G, Periaswamy B, Schlumberger MC, Rout S, et al. (2010) Enhanced CellClassifier: a multi-class classification tool for microscopy images. BMC Bioinformatics. 11: 30.
15. Harder N, Mora-Bermudez F, Godinez WJ, Wunsche A, Eils R, et al. (2009) Automatic analysis of dividing cells in live cell movies to detect mitotic delays and correlate phenotypes in time. Genome Res. 19: 2113–2124.
16. Jones TR, Carpenter AE, Lamprecht MR, Moffat J, Silver SJ, et al. (2009) Scoring diverse cellular morphologies in image-based screens with iterative feedback and machine learning. Proc. Natl. Acad. Sci. U. S. A. 106: 1826–1831.
17. Hoerl AE and Kennard R (1970) Ridge regression: biased estimation for nonorthogonal problems. Technometrics 12: 55–67.
18. Hastie T (2009) The Elements of Statistical Learning: Data Mining, Inference, and Prediction. Springer-Verlag. 43.

Cytotherapy, 2012; 14: 791–801

informa
healthcare

Characteristic differences among osteogenic cell populations of rat bone marrow stromal cells isolated from untreated, hemolyzed or Ficoll-treated marrow

HIDEKI AGATA[1], MIKA YAMAZAKI[1,2], MARIKO UEHARA[2], AKIKO HORI[1], YOSHINORI SUMITA[3], ARINOBU TOJO[4] & HIDEAKI KAGAMI[1,5]

[1]*Tissue Engineering Research Group, Division of Molecular Therapy, Advanced Clinical Research Center, The Institute of Medical Science, The University of Tokyo, Tokyo, Japan,* [2]*TES Holdings Corporation Ltd, Tokyo, Japan,* [3]*Department of Regenerative Oral Surgery, Unit of Translational Medicine, Nagasaki University Graduate School of Biomedical Sciences, Nagasaki, Japan,* [4]*Division of Molecular Therapy, Advanced Clinical Research Center, The Institute of Medical Science, The University of Tokyo, Tokyo, Japan, and* [5]*Department of Oral Maxillofacial Surgery, Matsumoto Dental University, Nagano, Japan*

Abstract

Background aims. Although bone marrow (BM) stromal cells (SC; BMSC) isolated from adherent cultures of untreated BM are known to contain both committed and uncommitted osteogenic cells, it remains unknown whether BMSC isolated either by hemolysis or Ficoll centrifugation also contain both of these populations. *Methods.* Differences in the osteogenic cell populations of rat BMSC isolated from untreated, hemolyzed or Ficoll-treated BM were analyzed by *in vivo* transplantation, flow cytometry, alkaline phosphatase (ALP) assay, real-time polymerase chain reaction (PCR) and alizarin red staining. *Results.* Transplantation of non-cultured samples indicated that the Ficolled BMSC contained the lowest number of committed osteogenic cells. Flow cytometric analysis of cultured, non-induced samples showed that the percentage of ALP-positive cells was significantly lower in Ficolled BMSC. Quantitative ALP assays confirmed that the lowest ALP activity was in the Ficolled BMSC. Hemolyzed BMSC also contained lower numbers of committed osteogenic cells than untreated BMSC, but still more than Ficolled BMSC. Interestingly, the Ficolled BMSC showed the greatest levels of osteogenic ability when cultured in osteogenic induction medium. *Conclusions.* These findings suggest that, although Ficolled BMSC rarely contain committed osteogenic cells, they are able to show comparable or even greater levels of osteogenic ability after induction, possibly because they contain a greater proportion of uncommitted stem cells. In contrast, induction is optional but recommended for both untreated and hemolyzed BMSC before use, because both these groups contain both committed and uncommitted osteogenic cells. These findings are of significant importance when isolating BMSC for use in bone tissue engineering.

Key Words: *bone marrow stromal cells, Ficoll, hemolysis, osteogenic cells, stem cells*

Introduction

Bone marrow (BM) stromal cells (SC; BMSC) isolated from adherent cultures of untreated whole BM (normal BMSC) contain an uncommitted stem cell population called mesenchymal stromal cells that can differentiate into multiple (osteogenic, chondrogenic, adipogenic, myogenic and neurogenic) lineages (1,2). It remains controversial regarding whether the multilineage differentiation ability of normal BMSC is attributed solely to uncommitted stem cells, because the BMSC population is composed of a heterogeneous collection of cells that might include committed progenitors of each lineage (3). Nonetheless, the osteogenic ability at least of normal BMSC depends on both committed and uncommitted cells, as it has long been known that normal BMSC contain committed osteogenic cells such as pre-osteoblasts (4).

Uncommitted stem cells require induction stimuli to promote osteogenic differentiation (5). Thus BMSC are generally cultured in osteogenic induction medium before use in bone tissue engineering. However, the induction process can be omitted or shortened when BMSC include large numbers of committed osteogenic cells, as committed cells spontaneously differentiate into osteoblasts (4,5). Thus the proportion of committed osteogenic cells affects both the protocol design as well as the total cost of bone tissue engineering. In addition, this

Correspondence: **Hideki Agata**, Tissue Engineering Research Group, Division of Molecular Therapy, Advanced Clinical Research Center, The Institute of Medical Science, The University of Tokyo, 4-6-1 Shirokanedai, Minato-ku, Tokyo, 108-8639, Japan. E-mail: agata@ims.u-tokyo.ac.jp

(Received 29 July 2011; accepted 4 March 2012)

ISSN 1465-3249 print/ISSN 1477-2566 online
DOI: 10.3109/14653249.2012.674639

proportion may significantly affect the osteogenic ability of BMSC, as highly osteogenic BMSC are able to form bone without induction (6). Therefore it is important to investigate the proportion of committed osteogenic cells when analyzing the osteogenic ability of BMSC, although few studies have focused on the importance of that population.

In general, BMSC are obtained from adherent cultures of untreated whole BM because they are able to form adherent colonies unlike non-adherent hematopoietic cells (7,8). However, this technique may be inefficient for the isolation of BMSC because untreated BM contains a large proportion of erythrocytes and their presence can interfere with the initial colony-forming ability of BMSC. Both density-gradient centrifugation over Ficoll® (GE Healthcare UK Ltd, Amersham, UK) and hemolysis treatment with ammonium chloride are techniques used for the removal of erythrocytes from BM to enhance BMSC adherence, and BMSC isolated by these techniques have been shown to possess multilineage differentiation abilities (9,10). However, it remains unknown whether these BMSC have the same differentiative potential as BMSC isolated from whole BM, as the cellular composition of BMSC may vary with the isolation techniques (11). Differences in cellular composition may greatly influence the osteogenic characteristics of BMSC, because the osteogenic ability of normal BMSC depends on at least two different cell populations, i.e. committed osteogenic cells and uncommitted stem cells (5). Therefore, it is important to investigate the osteogenic BMSC populations following isolation by either Ficoll fractionation or hemolysis before applying these techniques to bone tissue engineering. In the present study, we isolated BMSC from untreated, hemolyzed or Ficoll-treated rat BM and analyzed their differences in osteogenic cell populations, with a special emphasis on committed osteogenic cell populations.

Methods

BM isolation from Sprague–Dawley rats

Sprague–Dawley (SD) rats (Jcl. SD, male, 6 weeks old) were purchased from Clea Japan Inc. (Tokyo, Japan). All experiments were approved by the Animal Ethics Screening Committee of The Institute of Medical Science, The University of Tokyo (Tokyo, Japan). After intraperitoneal overdose administration of pentobarbital sodium, the femurs and tibiae were carefully dissected from the killed rats. The tips of the bones were cut with scissors to expose the BM. Thereafter, BM was flushed out from each bone by injecting 7.5 mL Hanks' balanced salt solutions (HBSS; Wako Pure Chemical Industries Ltd, Osaka, Japan) with an 18-gauge needle (Terumo, Tokyo, Japan) attached to a 20-mL syringe (Terumo), and collected in a 50-mL centrifuge tube (Becton Dickinson, Pharmingen, Franklin Lakes, NJ, USA). Then the tubes were centrifuged at 440 ***g*** for 5 min at 4°C. After discarding the supernatants, the marrow cells from each rat were resuspended in 10.5 mL Dulbecco's phosphate-buffered saline (DPBS; Nissui Pharmaceutical Co. Ltd, Tokyo, Japan) and divided among three different tubes (each tube containing 3.5 mL marrow cell suspensions).

Isolation of BMSC from untreated, hemolyzed or Ficoll-treated BM

To isolate BMSC, marrow cell suspensions were processed on Ficoll or hemolyzed as described elsewhere (9).

Ficoll-separated cells

For Ficoll treatment, 3.5-mL marrow cell suspensions were diluted with 7.5 mL DPBS and carefully laid over 15 mL Ficoll-Paque® (GE Healthcare UK Ltd). After centrifugation (400 ***g***, 30 min, 20°C), the mononuclear cell fraction was collected and moved to another new tube. Subsequently, cells were washed twice in DPBS. After centrifugation (400 ***g***, 10 min, 4°C), the supernatants were discarded and the cell pellets obtained were suspended in 1 mL physiologic saline (Otsuka Pharmaceutical Co. Ltd, Tokushima, Japan) for transplantation experiments or suspended in 6 mL α-MEM (Minimum Essential Medium Alpha) (Wako Pure Chemical Industries Ltd) supplemented with 10% fetal bovine serum (JRS, Woodland, CA, USA) and antibiotics/antimycotics for cell-culture analyzes. The suspensions were termed 'Ficolled cells'.

Hemolyzed cells

For hemolysis treatment, 3.5-mL marrow cell suspensions were mixed with 10 mL lysis buffer [0.15 M ammonium chloride (NH_4Cl; Sigma-Aldrich, St Louis, MO, USA), 10 mM potassium bicarbonate ($KHCO_3$; Sigma-Aldrich) and 0.1 mM ethylenediamine-*N*,*N*,*N*′,*N*′-tetraacetic acid, tetrasodium salt, tetrahydrate (EDTA·4Na; Dojindo Laboratories, Kumatomo, Japan)] and incubated for 10 min at room temperature on a horizontal shaker. Then the cells were centrifuged (400 ***g***, 10 min, 4°C) and washed twice in DPBS. After centrifugation (400 ***g***, 10 min, 4°C), the supernatants were discarded and the resultant cell pellets were suspended in 1 mL physiologic saline for the transplantation experiment, or suspended in 6 mL serum-containing medium for cell-culture analyzes.

Untreated group

As untreated controls, 3.5-mL marrow cell suspensions were washed twice in DPBS. After centrifugation (400 ***g***, 10 min, 4°C), the supernatants were discarded and the resultant cell pellets were suspended in 1 mL physiologic saline for transplantation experiments or suspended in 6 mL serum-containing medium for cell-culture analyzes.

Transplantation of non-cultured cells isolated by different techniques

Committed osteogenic cells spontaneously differentiate into bone-forming osteoblasts (5). Therefore non-cultured samples of untreated, hemolyzed or Ficolled cells were analyzed for their *in vivo* bone-forming abilities to investigate differences in committed osteogenic cells. Samples were transplanted to ectopic sites to avoid the effects of recipient nude mouse-derived osteogenic cells. One milliliter of saline containing each sample was mixed with 50 mg β-tricalcium phosphate (β-TCP) granules (G1 type OSferion®; Olympus Terumo Biomaterials, Tokyo, Japan) in a 14-mL polypropylene tube (Becton Dickinson) and centrifuged (100 ***g***, 5 min, 4°C). After careful removal of the supernatants, 100-μL 10 mg/mL fibrinogen solution (bovine plasma fibrinogen; F8630; Sigma-Aldrich) and 5-μL 100 U/mL thrombin solution (bovine plasma thrombin; T9549; Sigma-Aldrich) were added to each cell–β-TCP mixture to form a fibrin clot. Thereafter each clotted cell mixture was transplanted into the subcutaneous space on the backs of 6-week-old female BALB/CAJcl-nu/nu mice (Clea Japan Inc.) under anesthesia with pentobarbital sodium. Transplants were harvested 4 weeks after the operation.

Histologic assessment of the transplants of non-cultured samples

Harvested samples were fixed in 10% buffered formalin, decalcified in Kalkitox™, neutralized in 5% sodium sulfate solution (all purchased from Wako Pure Chemical Industries Ltd) and embedded in paraffin. Five-micrometer thick sections were prepared from the middle of each transplant and stained with hematoxylin and eosin (H&E).

Microscopic examination of H&E-stained sections was conducted to determine the number of transplants that contained ectopic bone formation. The percentage of successful ectopic bone formation (number of transplants containing ectopic bone/total transplants) was calculated to assess the bone-forming potential of untreated, hemolyzed and Ficolled cells, as described elsewhere (12). To investigate the bone-forming activity, light microscopic images were captured with a digital camera (Carl Zeiss Japan, Tokyo, Japan) and transferred to a computer. Then the percentage of the area containing bone (new bone area/total area) was assessed manually using Image J (Scion Corporation, Frederick, MD, USA), as described elsewhere (13). The extent of bone formation in each transplant was scored on a semi-quantitative scale in a manner similar to that described previously (14). For example, sections prepared from the middle of each transplant were scored on a scale of 0 to 3: a score of 0 corresponded to no bone formation, while a score of 3 corresponded to abundant bone formation (bone area > 10%) (Table I). Thereafter, the average bone score of the transplants (total bone score/total transplants) was calculated for each group.

In vitro *expansion of BMSC isolated from untreated, hemolyzed or Ficoll-treated marrow cell suspensions*

For further investigations, cells isolated from untreated, hemolyzed or Ficoll-treated marrow cell suspensions were resuspended in 6 mL serum-containing medium for culture expansion as described above. Cells were plated in 3-mL/well volumes in 6-well plates (Becton Dickinson) and maintained in a 37°C, 5% CO_2 incubator. On the following day, the culture medium was replaced with fresh medium of the same type. Adherent cells were re-fed with fresh medium on the fourth day. After 1 week of culture, adherent cells were treated with 0.5% trypsin–EDTA (Invitrogen, Carlsbad, CA, USA), and cells detached within 3 min were passaged and replated in 100-mm tissue culture dishes (TPP Techno Plastic Products AG, Trasadingen, Switzerland) at a density of 6.5×10^3 cells/cm^2 for flow cytometric analyses, or replated into multiwell plates (Becton Dickinson) for other analyzes.

Flow cytometric analysis

Differences in cell-surface marker expression were analyzed with a fluorescent-activated cell sorter (FACS) Aria flow cytometer (Becton Dickinson). Fluorescence isothiocyanate (FITC)-conjugated, phycoerythrin (PE)-conjugated, or allophycocyanin (APC)-conjugated antibodies targeted against CD45, CD54, CD90 (all from Biolegend, San Diego, CA,

Table I. Semi-quantitative scale to estimate the extent of bone formation.

	Bone score (Extent of bone formation in transplant)
0	No bone evident
1	Low bone formation (bone area < 5%)
2	Moderate bone formation (5% < bone area < 10%)
3	Abundant bone formation (bone area > 10%)

USA) and a biotinylated antibody against alkaline phosphatase (ALP; BAM1448; R&D Systems Inc., Minneapolis, MN, USA) were used for the analyzes. The biotinylated antibody was detected with a streptavidin–FITC conjugate (Biolegend). Propidium iodide (Dojindo) was used to detect dead cells.

First-passage cells were detached with trypsin–EDTA and 1×10^6 cells were resuspended in 50 μL ice-cold DPBS. Cells were then incubated with individual antibodies for 20 min on ice. Thereafter, cells were washed and incubated with a streptavidin conjugate for 20 min on ice. Finally, the cells were washed, resuspended in 200 μL ice-cold DPBS, stained with propidium iodide, and analyzed. Data analysis was performed using FlowJo software (TreeStar Inc., San Carlos, CA, USA).

Fluorescent immunostaining

Fluorescent immunostaining of CD45 and CD54 was performed to confirm the results of flow cytometric analyzes. First-passage cells were plated in 24-well plates at a density of 5×10^4 cells/well in serum-containing medium, and cultured until 70% confluent. Thereafter, cells were fixed with 4% paraformaldehyde, washed three times with DPBS, and treated with 100 mM glycine buffer. Then the cells were washed again three times and incubated with biotinylated antibodies against CD45 or CD54 (both 1:200 dilutions; Biolegend) at 4°C overnight. The next day, cells were rewashed three times and incubated with a streptavidin–FITC conjugate (1:800 dilutions; Biolegend) for 20 min at room temperature. After three washes with DPBS, cells were counterstained with Vectashield-mounting medium with DAPI (Vector Laboratories Inc., Burlingame, CA, USA) and observed under a fluorescence microscope (Axio Obserber Z-1; Carl Zeiss Japan). Digital images were acquired using an AxioCam HRm and AxioVision software (Carl Zeiss Japan).

Cell-number analysis and quantitative ALP assay

Cell-number analyzes and quantitative ALP assays were performed as described elsewhere with modifications (13). First-passage cells from each group were plated into 24-well plates at a density of 2×10^4 cells/well in serum-containing medium. The next day, cells were fed with non-induction medium (serum-containing medium) or osteogenic induction medium [serum-containing medium with 10 nM dexamethasone (Sigma-Aldrich), 100 μM ascorbic acid (Wako Pure Chemical Industries Ltd.), and 10 mM glycerol 2-phosphate disodium salt hydrate (β-glycerophosphate; Sigma-Aldrich)]. Culture medium was replaced with fresh medium twice a week. After 1 or 2 weeks of culture, cell-number analyzes and quantitative ALP assays were performed with a commercially available *p*-nitrophenyl phosphate tablet set (Sigma-Aldrich) and a cell-counting kit-8 (WST-8®; Dojindo).

Briefly, 50 μL WST-8 were added to each well containing 0.5 mL fresh medium, incubated for 60 min, and absorbance was read at 450 nm to assess cell numbers. After WST-8 analysis, each well was washed twice with DPBS and 400 μL *p*-nitrophenyl phosphate solution was added to each well. After 10 min of incubation at 37°C, the conversion to *p*-nitrophenol was stopped with 400 μL 3N NaOH and the absorbance of *p*-nitrophenol was measured at 405 nm. ALP activity was expressed as *p*-nitrophenol absorbance ((Optical Density OD); 405 nm)/WST-8 absorbance (OD; 450 nm).

Real-time quantitative polymerase chain reaction

Real-time quantitative polymerase chain reaction (real-time qPCR) was conducted to investigate differences in the expression of osteogenic marker genes. Second-passage cells from each group were plated in 6-well plates at a density of 1×10^5 cells/well in serum-containing medium. The next day, cells were fed with non-induction medium (serum-containing medium) or osteogenic induction medium. Culture medium was replaced with fresh medium twice a week. After 1 or 2 weeks of culture, total RNA was extracted with an RNeasy® Mini Kit (QIAGEN Science, Germantown, MD, USA). First-strand cDNA syntheses were performed with a PrimeScript® RT Master Mix (Perfect Real Time) (Takara Bio Inc., Shiga, Japan). Real-time qPCR was conducted using the primers for osteopontin (forward, gatgaaccaagcggtggaaac; reverse, tgaaactcgtggctctgatg), core-binding factor subunit alpha-1 (Cbfa-1; forward, gccaggttcaacgatctgag; reverse, gaggcggtcagagaacaaac), osteocalcin (forward, agctcaaccccaattgtgac; reverse, agctgtgccgtccatacttt) and glyceraldehyde 3-phosphate dehydrogenase (GAPDH; forward, aactcccattcctccaacctt; reverse, gagggcctctctcttgctct), which have been described previously (15). A SYBR® Premix ExTaq™ II (Tli RNase H Plus) (Takara Bio Inc.) was used for real-time qPCR according to the manufacturer's instructions. The reactions were performed with a Thermal Cycler Dice® Real Time System II (Takara Bio Inc.) at 95°C for 30 s, and then 40 cycles at 95°C for 5 s and 60°C for 1 min. The cycle threshold (Ct) values were calculated by the second derivative maximum method, and the relative quantities were calculated based on a standard curve generated with serial dilutions of cDNA. GAPDH was used as an internal control.

In vitro *mineralization assays*

To investigate differences in the mineralizing potentials of BMSC, second-passage cells from each group were plated in 24-well plates at a density of 5×10^4 cells/well in serum-containing medium. The next day, cells were fed with non-induction medium (serum-containing medium) or osteogenic induction medium. Culture medium was replaced with fresh medium twice a week. After 3 weeks of culture, cells were fixed with 70% ethanol at –20°C for 60 min, washed, and stained for 15 min with a saturated solution of alizarin red S (pH 4.2; Sigma-Aldrich), as described elsewhere (16).

Statistical analysis

Data are presented as the mean ± standard deviation. Multiple comparisons were performed with one-way ANOVA and protected Fisher's least significant difference test. Differences were considered statistically significant when $P < 0.01$ or $P < 0.05$.

Results

Cell isolation by each method

The same quantities of marrow cells were processed by either Ficoll-Paque centrifugation (Ficolled cells) or hemolysis buffer (hemolyzed cells), or were left without treatment (untreated cells) (Figure 1A). After each treatment, the viable cell number was counted using a Countess® automated cell counter (Invitrogen) following the manufacturer's instructions, with fixed settings (sensitivity 2; size gating 10–60 μm; circularity 85%). The average number of isolated cells was greatest in the untreated fractions, followed by hemolyzed fractions, and lowest in Ficolled fractions (Figure 1B).

Bone-forming ability of non-cultured samples of untreated, hemolyzed and Ficoll-treated marrow

The fraction of successful ectopic bone transplants was defined as the percentage of transplants containing ectopic bone/total transplants. Following transplants of untreated, hemolyzed or Ficolled cells, the successful transplants were assessed as 86%, 57% and 43%, respectively (Figure 2A). The average bone scores (total bone score/the number of transplants) were 1.14, 0.86 and 0.43, respectively (Figure 2B). Representative histologic photographs are shown in Figure 2C–E (C, untreated cells; D, hemolyzed cells; E, Ficolled cells).

Flow cytometric analysis of cell-surface marker expression in cultured BMSC isolated by each method

Expression profiles of cell-surface markers of hematopoietic cells (CD45), mesenchymal cells

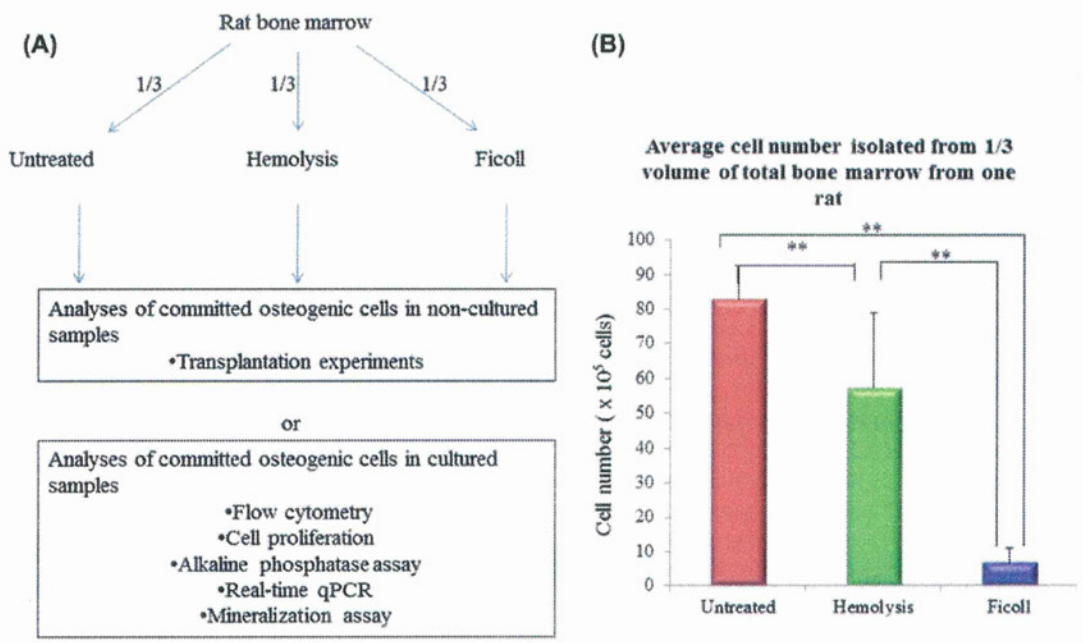

Figure 1. Experimental design and the average number of cells isolated from untreated, hemolyzed or Ficoll-treated BM. (A) Experimental design of this study. Rat BM was divided into three portions and the suspensions were hemolyzed, subjected to Ficoll fractionation or left without treatment (untreated). Thereafter, cells obtained by each method were analyzed for differences in osteogenic cell populations with or without *in vitro* cultivation. (B) Average yield of cells from untreated, hemolyzed and Ficolled BM. Significant differences were observed in the average numbers of isolated cells among the groups. Data are presented as the mean ± standard deviation ($n = 6$). $^{**}P < 0.01$.

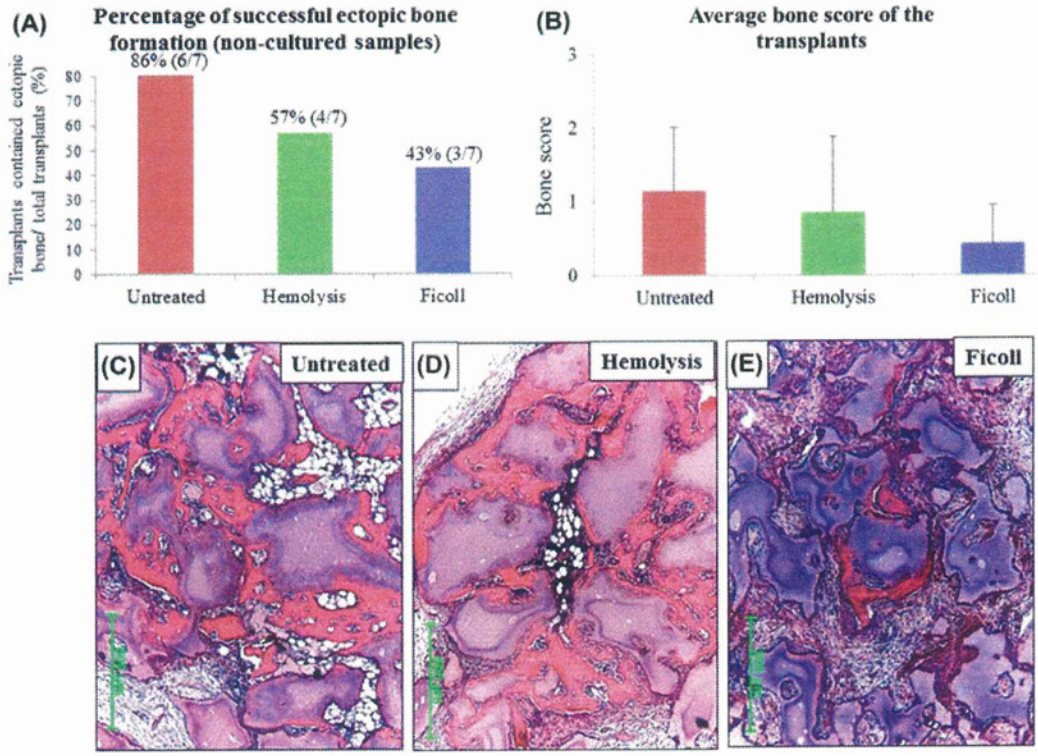

Figure 2. Bone-forming ability of non-cultured samples. (A) Successful ectopic bone formation (transplants containing bone/total transplants) of non-cultured samples, which was calculated from the results of seven independent experiments, was greatest in the untreated group, followed by the hemolyzed group, and lowest in the Ficolled group. (B) The average bone score (total bone score/total transplants) was greatest in the hemolyzed group, followed by the untreated group, and lowest in the Ficolled group ($n = 7$). Representative histology of the transplants of non-cultured samples from untreated (C), hemolyzed (D) and Ficolled (E) fractions. Transplants of the Ficolled fraction formed lower amounts of new bone than those of the other groups. Green scale bar: 100 μm. color images are available online

(CD54 and CD90) and committed osteogenic cells (ALP) were analyzed by flow cytometry. Flow cytometric analyzes were performed three times and representative expression profiles of cultured, non-induced samples from each group are shown in Figure 3. The percentages of CD45-positive cells in untreated, hemolyzed and Ficolled cells were 20%, 17% and 28%, respectively. Thus there appeared to be no significant differences in the proportions of hematopoietic cells among the groups (Figure 3). Expression profiles of CD54 and CD90, both of which are expressed by mesenchymal cells as well as some hematopoietic cells such as monocytes and dendritic-like cells (17), did not show significant differences among the groups (Figure 3). In contrast, there was a significant difference in the expression of ALP. The percentages of ALP-positive cells in untreated, hemolyzed and Ficolled cells were 41%, 41% and 7%, respectively. Thus the Ficolled cells might contain a lower proportion of committed osteogenic cells than the other isolates (Figure 3).

Expression of CD45 and CD54 in cultured BMSC assessed by immunostaining

Fluorescent immunostaining of CD45 and CD54 was performed to confirm the expression of these cell-surface markers in cultured BMSC. In accordance with the results of flow cytometric analyzes, approximately 20% of the cells were positive for CD45 (Figure 4A–D), while 100% of the cells were positive for CD54 (Figure 5A–D).

Cell proliferation and ALP activities in non-induction medium or osteogenic induction medium

Differences in cell proliferation and ALP activities when cultured in non-induction medium or osteogenic induction medium were analyzed quantitatively. As shown in Figure 6A, B, all cell groups showed greater cell proliferation in non-induction medium. Although the Ficolled cells showed relatively slower proliferation regardless of the type of medium, no significant differences were observed

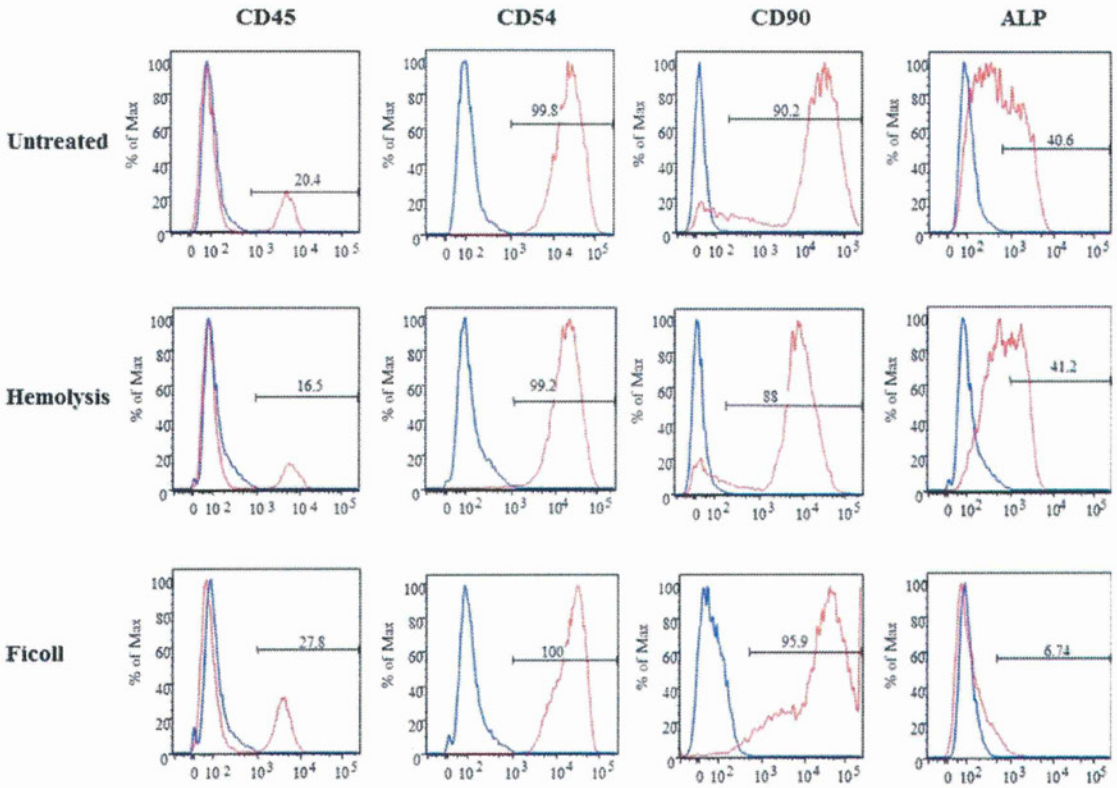

Figure 3. Expression profiles of cell-surface antigens of BMSC grown from each fraction. BMSC from each fraction were expanded in non-induction medium and analyzed by flow cytometry to investigate differences in the expression of CD45, CD54, CD90 and ALP. The percentage of ALP-positive cells was significantly lower in the Ficolled fraction, although no significant difference was observed in the expression profiles of other cell-surface markers among the isolates. Blue line: unstained control cells.

among the groups at any sampling point. As for ALP activity, a statistically significant difference was observed after 14 days of culture in non-induction medium. The ALP activity of non-induced Ficolled cells was significantly lower than that of the other isolates (Figure 6C), in accordance with the results of flow cytometric analyzes. Notably, the Ficolled group showed the greatest levels of ALP activity when

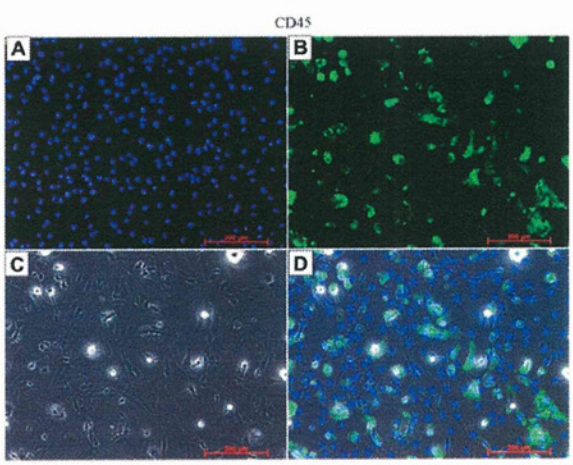

Figure 4. Fluorescent immunostaining of CD45 in BMSC grown from untreated BM. Fluorescent immunostaining of CD45 was performed to confirm the results of flow cytometric analyzes. Approximately 20% of cells grown from untreated BM were positive for CD45, even at passage 1. (A) DAPI, (B) FITC–CD45, (C) phase–contrast, (D) merged image of DAPI, FITC–CD45 and phase–contrast photographs.

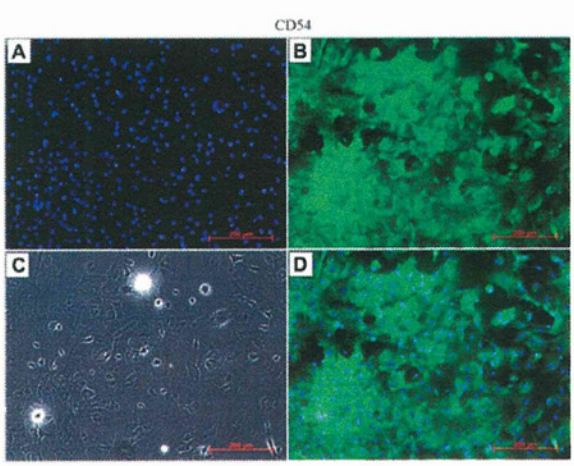

Figure 5. Fluorescent immunostaining of CD54 in BMSC grown from untreated BM. Fluorescent immunostaining of CD54 was performed to confirm the results of flow cytometric analyzes. Cells grown from untreated BM were 100% positive for CD54. (A) DAPI, (B) FITC–CD54, (C) phase–contrast, (D) merged image of DAPI and FITC–CD54.

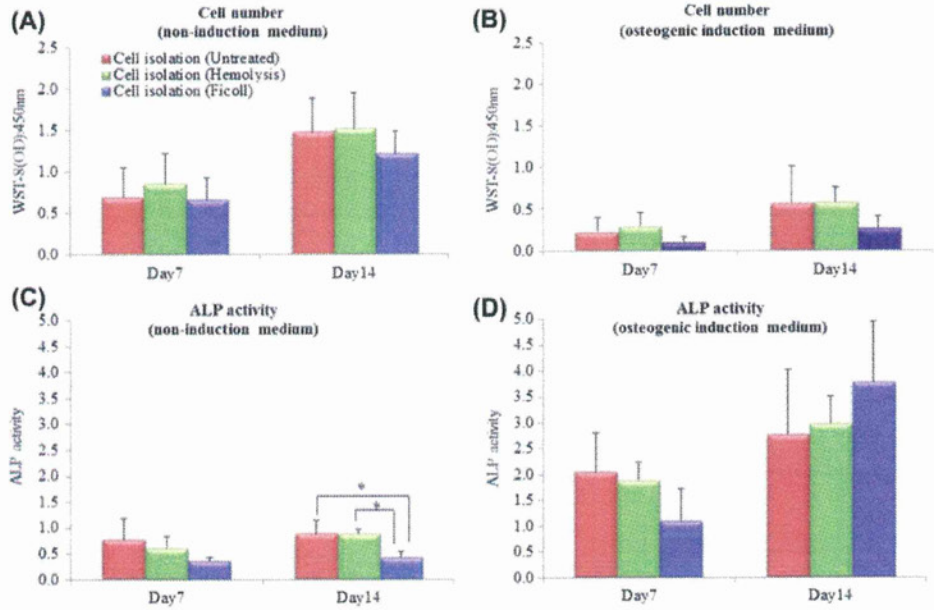

Figure 6. Cell proliferation and ALP activities in non-induction medium or osteogenic induction medium. BMSC grown from untreated, hemolyzed or Ficolled BM were cultured in non-induction medium or osteogenic induction medium and analyzed for differences in cell proliferation and ALP activities. (A) Cell proliferation in non-induction medium. All fractions proliferated similarly in non-induction medium and no significant differences were observed in cell number at either 7- or 14-day sampling points. (B) Cell proliferation in osteogenic induction medium. All fractions proliferated similarly and no significant differences were observed in cell number at either sampling point, although cell proliferation in osteogenic induction medium was significantly lower than that in non-induction medium. (C) ALP activity in non-induction medium. A statistically significant difference was observed in ALP activities between Ficolled cells and the other fractions after 14 days of culture in non-induction medium. (D) ALP activity in osteogenic induction medium. Although all fractions showed greater ALP activity than in non-induction medium, the Ficolled fraction showed the lowest ALP activity at the 7-day sampling point. However, this fraction showed the greatest ALP activity at the 14-day sampling point. Data are presented as the mean±standard deviation ($n=3$). $^{*}P<0.05$.

cultured in osteogenic induction medium for 14 days, although the difference did not reach a statistically significant level (Figure 6D).

Expression of osteogenesis-related genes in non-induction medium or osteogenic induction medium

Differences in the expression of osteogenesis-related genes (osteopontin, Cbfa-1 and osteocalcin) were analyzed by real-time qPCR. The expression of osteopontin after 7 days of culture both in non-induction medium and in osteogenic induction medium was lowest in the Ficolled group, although this group showed the greatest osteopontin expression after 14 days of culture in osteogenic induction medium (Figure 7A,B). While the expression of Cbfa-1 was also relatively low in the Ficolled group when cultured in non-induction medium (Figure 7C), this group showed the greatest Cbfa-1 expression after 14 days of culture in osteogenic induction medium (Figure 7D), as observed in osteopontin expression (Figure 7B). The Ficolled group also showed the greatest osteocalcin expression after 14 days of culture in osteogenic induction medium (Figure 7F), although the expression of osteocalcin in this group was relatively high even when cultured in non-induction medium (Figure 7E).

In vitro *mineralization ability*

Differences in *in vitro* mineralization abilities were analyzed by alizarin red staining. As shown in Figure 8, all groups showed *in vitro* mineralization ability after 21 days of culture in osteogenic induction medium. The intensities of the alizarin red staining were comparable among the groups.

Discussion

Committed osteogenic cells are usually classified into three types, i.e. osteoprogenitors, pre-osteoblasts and osteoblasts, according to their stage of differentiation. All of these osteogenic cells possess bone-forming ability without osteogenic induction (18,19). Accordingly, we first investigated differences in the bone-forming ability of non-cultured samples of untreated, hemolyzed and Ficoll-fractionated BM. As shown in Figure 2A,B, following transplantation

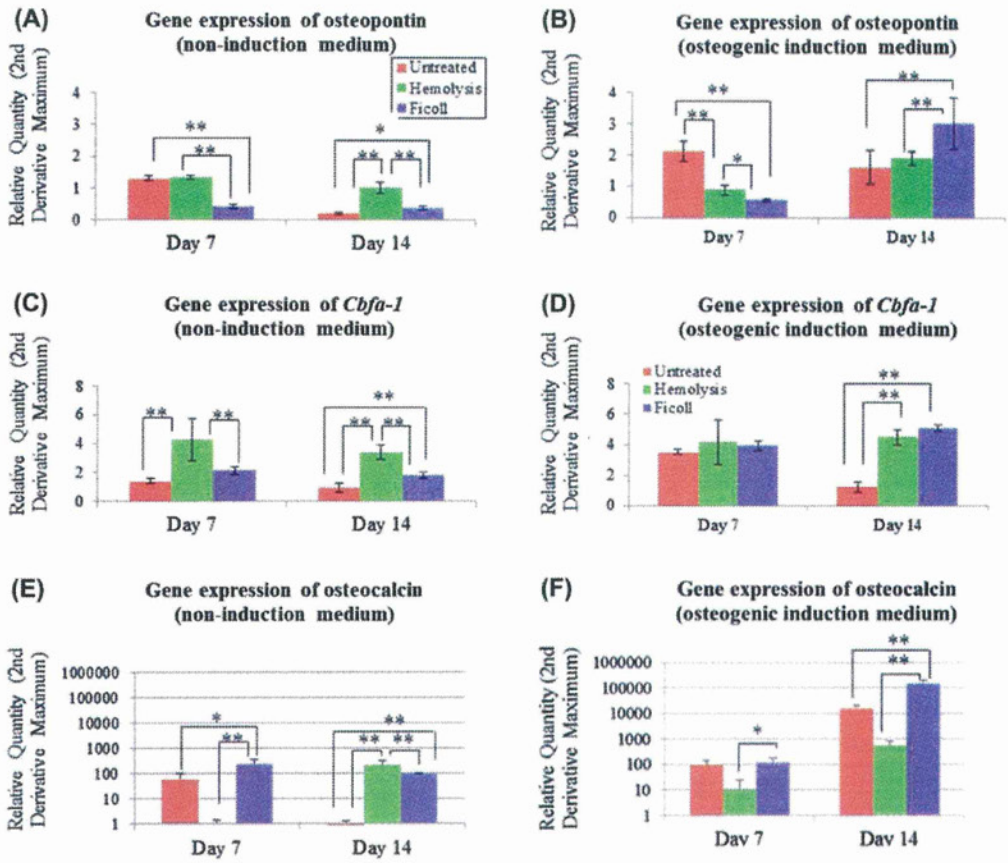

Figure 7. Expression of osteogenesis-related genes in non-induction medium or osteogenic induction medium. BMSC grown from untreated, hemolyzed or Ficolled BM were cultured in non-induction medium or osteogenic induction medium and analyzed for differences in gene expression of osteopontin, Cbfa-1 and osteocalcin. (A) The expression of osteopontin when cultured in non-induction medium. (B) Osteopontin expression in osteogenic induction medium. The Ficolled fraction showed the greatest expression after 14 days of culture. (C) The expression of Cbfa-1 when cultured in non-induction medium. (D) Cbfa-1 expression in osteogenic induction medium. The Ficolled fraction showed the greatest expression after 14 days of culture. (E) The expression of osteocalcin when cultured in non-induction medium. (F) Osteocalcin expression in osteogenic induction medium. The Ficolled fraction showed the greatest expression after 14 days of culture. Data are presented as the means ± standard deviation (n = 3). $^{*}P < 0.05$, $^{**}P < 0.01$.

the percentages of successful ectopic bone formation and the average bone scores were greatest in the untreated group and lowest in the Ficolled group, suggesting that Ficolled BM contained the lowest number of committed osteogenic cells. As for the hemolyzed group, the percentage of transplants successfully achieving ectopic bone formation was lower (Figure 2A) but the average bone score was comparable with the untreated group (Figure 2B), suggesting that hemolyzed BM contain greater numbers of committed osteogenic cells than the Ficolled BM.

To investigate further differences in committed osteogenic cell populations, cells from each group were cultivated *in vitro* in non-induction medium and analyzed for differences in the percentages of ALP-positive cells by flow cytometry. This approach was utilized because cell-surface ALP expression as well as bone-forming ability are important characteristics of committed osteogenic cells (20,21). As shown in Figure 3, the percentage of ALP-positive cells was significantly lower in Ficolled cells, although no significant differences were observed in the expression profiles of other cell-surface markers (CD45, CD54 and CD90) among the groups, indicating that Ficolled cells were characteristically different from the other groups in the proportion of committed osteogenic cells. Quantitative ALP assays also provided supportive evidence that Ficolled cells included a lower proportion of committed osteogenic cells than the other fractions (Figure 6C), although cell number and growth were comparable among the groups (Figure 6A). On the other hand, no significant differences were observed between untreated and hemolyzed fractions in these assays, suggesting that cultured BMSC from both untreated and hemolyzed BM contained similar proportions of committed osteogenic cells.

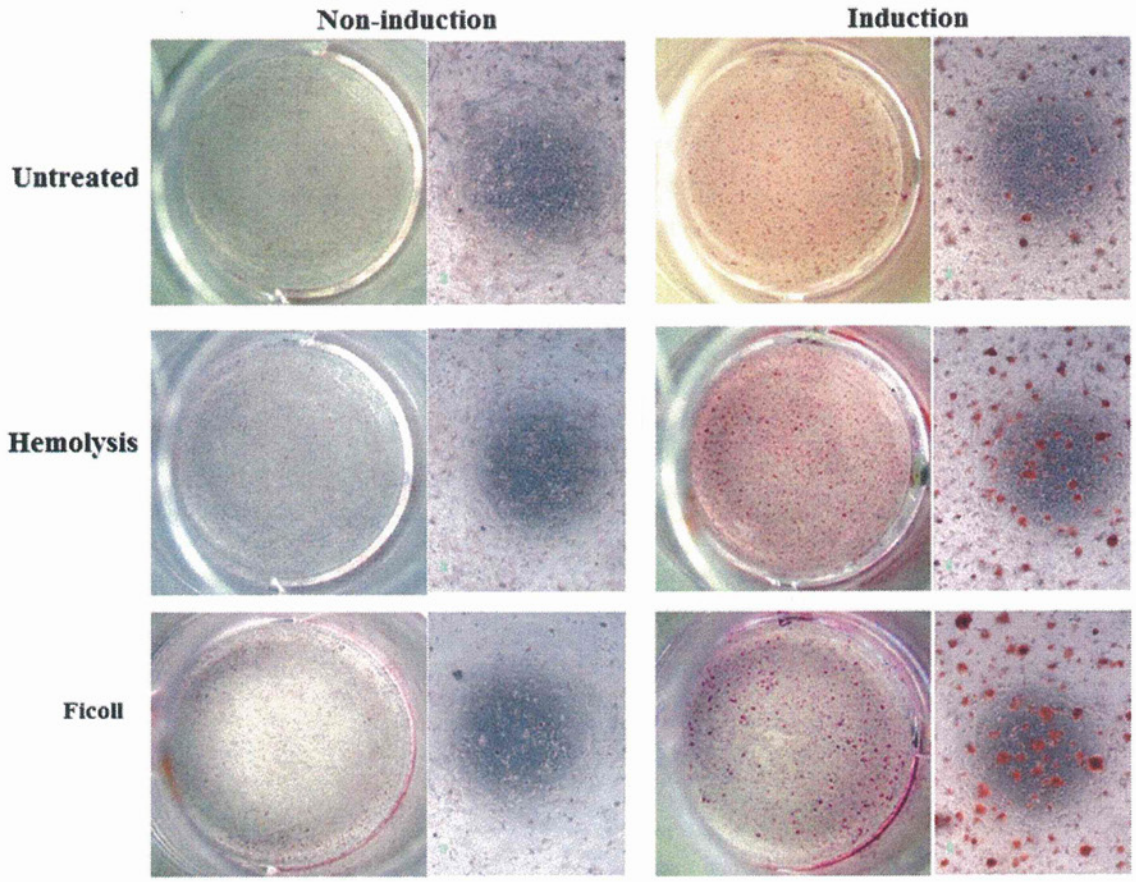

Figure 8. Alizarin red staining after 21 days of culture in non-induction medium or osteogenic induction medium. BMSC grown from untreated, hemolyzed or Ficolled BM were cultured in non-induction medium or osteogenic induction medium for 21 days and analyzed for differences in *in vitro* mineralization ability by alizarin red staining. In non-induction medium, *in vitro* mineralization was not observed in any groups. In contrast, all groups showed comparable levels of calcified nodule formation in osteogenic induction medium.

Although these data suggest that the proportion of committed osteogenic cells is significantly lower in Ficolled cells, it remains unknown whether the osteogenic capacity of Ficolled cells is actually inferior to that of other fractions, because Ficolled cells are known to contain uncommitted stem cells (22). Therefore, we investigated the osteogenic ability of each group's BMSC when cultured in osteogenic induction medium by analyzing the level of ALP activity. As shown in Figure 6C, D, all induced samples showed greater levels of ALP activities than non-induced samples, suggesting that all groups contained uncommitted stem cells that required osteogenic induction to differentiate into that lineage. Interestingly, the ALP activity of the Ficoll-separated fraction was greater than that of other groups after 14 days of culture in osteogenic induction medium, although the difference did not reach a statistically significant level (Figure 6D). These results indicate that although Ficolled cells contain a lower proportion of committed osteogenic cells, this fraction shows greater or at least comparable levels of osteogenic ability when cultured in osteogenic induction medium, possibly because the Ficolled group contains a greater proportion of uncommitted stem cells. To support this, Ficolled cells showed the greatest gene expression of osteopontin, Cbfa-1 and osteocalcin after 14 days of culture in osteogenic induction medium (Figure 7B, D, E), and they were able to form calcified nodules after 21 days of culture in the induction medium, like untreated and hemolyzed fractions (Figure 8). Therefore, Ficolled cells should be induced before use in bone tissue engineering. In contrast, both untreated and hemolyzed groups could be used without osteogenic induction because both these groups contain committed osteogenic cells. However, it might be better to induce them before use in bone tissue engineering, because their osteogenic abilities also depend on uncommitted stem cells.

The hemolysis treatment of BM is useful for the efficient isolation of BMSC (9,10). In fact, the cell yield (harvested cell number after primary culture/days of primary culture/initially seeded cell number) calculated for untreated, hemolyzed and Ficolled groups was 0.44, 0.52 and 0.13, respectively. However, this study indicates that some of the committed osteogenic cells contained in BM are lost or damaged during the hemolysis treatment, because the percentage of successful ectopic bone formation was lower in the hemolyzed group than the untreated group. Thus it might be advisable to use adherent culture of untreated BM to isolate BMSC for use in bone tissue engineering. As for the Ficoll centrifugation technique, this study revealed that the osteogenic cell population obtained by Ficoll fractionation significantly differs from untreated and hemolyzed populations. As Ficolled cells rarely include committed osteogenic cells, this group is less osteogenic than other groups in the absence of induction. However, when cultured in osteogenic induction medium, the Ficolled fraction shows osteogenic ability comparable with the other fractions, possibly because this group contains a greater proportion of uncommitted stem cells. Therefore the Ficoll technique might be rather suitable for the isolation of multipotent BMSC. These findings should be taken into account when applying either Ficoll separation or hemolysis for the isolation of BMSC; it is better to select an isolation technique specific for the intended purpose.

Acknowledgments

The authors thank Olympus Terumo Biomaterials for providing G1 type OSferion®. This work was supported in part by a grant-in-aid (KAKENHI) for Young Scientist A from the Japan Society for the Promotion of Science and by a grant from TES Holdings Co. Ltd (Japan).

Disclosure of interest: The authors have no conflict of interests.

References

1. Bruder SP, Fink DJ, Caplan AI. Mesenchymal stem cells in bone development, bone repair, and skeletal regeneration therapy. J Cell Biochem. 1994;56:283–94.
2. Jiang Y, Vaessen B, Lenvik T, Blackstad M, Reyes M, Verfaillie CM. Multipotent progenitor cells can be isolated from postnatal murine bone marrow, muscle, and brain. Exp Hematol. 2002;30:896–904.
3. Ashton BA, Allen TD, Howlett CR, Eaglesom CC, Hattori A, Owen M. Formation of bone and cartilage by marrow stromal cells in diffusion chambers in vivo. Clin Orthop Relat Res. 1980;151:294–307.
4. Aubin JE, Liu F, Malaval L, Gupta AK. Osteoblast and chondroblast differentiation. Bone. 1995;17:77S–83S.
5. Aubin JE. Osteoprogenitor cell frequency in rat bone marrow stromal populations: role for heterotypic cell–cell interactions in osteoblast differentiation. J Cell Biochem. 1999;72:396–410.
6. Mendes SC, Tibbe JM, Veenhof M, Bakker K, Both S, Platenburg PP, et al. Bone tissue-engineered implants using human bone marrow stromal cells: effect of culture conditions and donor age. Tissue Eng. 2002;8:911–20.
7. McCulloch CA, Strugurescu M, Hughes F, Melcher AH, Aubin JE. Osteogenic progenitor cells in rat bone marrow stromal populations exhibit self-renewal in culture. Blood. 1991;77:1906–11.
8. Leboy PS, Beresford JN, Devlin C, Owen ME. Dexamethasone induction of osteoblast mRNAs in rat marrow stromal cell cultures. J Cell Physiol. 1991;146:370–8.
9. Horn P, Bork S, Diehlmann A, Walenda T, Eckstein V, Ho AD, et al. Isolation of human mesenchymal stromal cells is more efficient by red blood cell lysis. Cytotherapy. 2008;10:676–85.
10. Peterbauer-Scherb A, van Griensven M, Meinl A, Gabriel C, Redl H, Wolbank S. Isolation of pig bone marrow mesenchymal stem cells suitable for one-step procedures in chondrogenic regeneration. J Tissue Eng Regen Med. 2010;4:485–90.
11. Wagner W, Ho AD. Mesenchymal stem cell preparations: comparing apples and oranges. Stem Cell Rev. 2007;3:239–48.
12. Agata H, Asahina I, Watanabe N, Ishii Y, Kubo N, Ohshima S, et al. Characteristic change and loss of in vivo osteogenic abilities of human bone marrow stromal cells during passage. Tissue Eng Part A. 2010;16:663–73.
13. Agata H, Watanabe N, Ishii Y, Kubo N, Ohshima S, Yamazaki M, et al. Feasibility and efficacy of bone tissue engineering using human bone marrow stromal cells cultivated in serum-free conditions. Biochem Biophys Res Commun. 2009;382:353–8.
14. Mankani MH, Kuznetsov SA, Avila NA, Kingman A, Robey PG. Bone formation in transplants of human bone marrow stromal cells and hydroxyapatite-tricalcium phosphate: prediction with quantitative CT in mice. Radiology. 2004;230:369–76.
15. Kuroda S, Virdi AS, Dai Y, Shott S, Sumner DR. Patterns and localization of gene expression during intramembranous bone regeneration in the rat femoral marrow ablation model. Calcif Tissue Int. 2005;77:212–25.
16. Agata H, Kagami H, Watanabe N, Ueda M. Effect of ischemic culture conditions on the survival and differentiation of porcine dental pulp-derived cells. Differentiation. 2008;76:981–93.
17. Chen-Woan M, Delaney CP, Fournier V, Wakizaka Y, Murase N, Fung J, et al. *In vitro* characterization of rat bone marrow-derived dendritic cells and their precursors. J Leukoc Biol. 1996;59:196–207.
18. Włodarski KH. Properties and origin of osteoblasts. Clin Orthop Relat Res. 1990;252:276–93.
19. Aubin JE. Bone stem cells. J Cell Biochem. 1998;Suppl 30–31:73–82.
20. Herbertson A, Aubin JE. Cell sorting enriches osteogenic populations in rat bone marrow stromal cell cultures. Bone. 1997;21:491–500.
21. Kotobuki N, Matsushima A, Kato Y, Kubo Y, Hirose M, Ohgushi H. Small interfering RNA of alkaline phosphatase inhibits matrix mineralization. Cell Tissue Res. 2008;332:279–88.
22. Polisetti N, Chaitanya VG, Babu PP, Vemuganti GK. Isolation, characterization and differentiation potential of rat bone marrow stromal cells. Neurol India. 2010;58:201–8.